The Astrophysical Journal, 695:276–286, 2009 April 10 doi:10.1088/0004-637X/695/1/276

A SEARCH FOR H_2O MEGAMASERS IN HIGH-z TYPE-2 ACTIVE GALACTIC NUCLEI

Nicola Bennert[1,6], Richard Barvainis[2,3,7], Christian Henkel[4], and Robert Antonucci[5]
[1] Institute of Geophysics and Planetary Physics, University of California, Riverside, CA 92521, USA; bennert@physics.ucsb.edu
[2] National Science Foundation, 4301 Wilson Boulevard, Arlington, VA 22230, USA; rbarvai@nsf.gov
[3] Department of Physics, Gettysburg College, 300 North Washington Street, Gettysburg, PA 1732, USA
[4] Max-Planck-Institut für Radioastronomie, Auf dem Hügel 69, D-53121 Bonn, Germany; chenkel@mpifr-bonn.mpg.de
[5] Department of Physics, University of California, Santa Barbara, CA 93106, USA; ski@physics.ucsb.edu
Received 2008 September 22; accepted 2009 January 13; published 2009 March 30

ABSTRACT

We report a search for H_2O megamasers in 274 SDSS type-2 active galactic nuclei (AGNs; $0.3 < z < 0.83$), half of which can be classified as type-2 quasi-stellar objects (QSOs) from their [O III] 5007 luminosity, using the Robert C. Byrd Green Bank Telescope (GBT) and the Effelsberg 100 m radio telescope. Apart from the detection of the extremely luminous water vapor megamaser SDSS J080430.99+360718.1, already reported by Barvainis & Antonucci, we do not find any additional line emission. This high rate of nondetections is compared to the water maser luminosity function created from the 78 water maser galaxies known to date and its extrapolation toward the higher luminosities of "gigamasers" that we would have been able to detect given the sensitivity of our survey. The properties of the known water masers are summarized and discussed with respect to the nature of high-z type-2 AGNs and megamasers in general. In the Appendix, we list 173 additional objects (mainly radio galaxies, but also QSOs and galaxies) that were observed with the GBT, the Effelsberg 100 m radio telescope, or Arecibo Observatory without leading to the detection of water maser emission.

Key words: galaxies: active – galaxies: Seyfert – masers – quasars: general

Online-only material: machine-readable tables

1. INTRODUCTION

The 22 GHz H_2O maser emission line is of great astrophysical interest for its extreme requirements for density ($>10^7$ cm^{-3}), temperature (>300 K), and of course radial velocity coherence. It is detected in both Galactic and extragalactic star-forming regions and in the central regions of active galactic nuclei (AGNs). In AGNs, isotropic luminosities commonly reach values of $L_{H_2O} > 10L_\odot$ and the objects are then classified as "megamasers" (see recent reviews by e.g., Greenhill 2004; Morganti et al. 2004; Henkel et al. 2005b; Lo 2005).

So far, water megamaser emission has been detected in about 10% of AGNs surveyed in the local universe (Braatz et al. 2004). The association of water megamasers with AGNs of primarily Seyfert-2 or low-ionization nuclear emission-line region (LINER) type (Braatz et al. 1997, 2004) and the fact that the emission often arises from the innermost parsec(s) of their parent galaxy have raised great interest in the study of 22 GHz maser emission. It suggests that the so-far poorly constrained excitation mechanism is closely related to AGN activity, probably irradiation by X-rays (e.g., Neufeld et al. 1994). For Seyfert-2 galaxies, in the framework of the so-called unified model (Antonucci 1993), a dusty molecular disk or torus is seen edge-on where the conditions and velocity-coherent path lengths are favorable for the formation of megamaser activity.

In those cases in which the emission arises from a nuclear disk and can be resolved spatially using Very Long Baseline Interferometry (VLBI), the central black hole (BH) mass can be constrained, as has been successfully shown for NGC 4258 (e.g., Greenhill et al. 1995; Miyoshi et al. 1995; Herrnstein et al. 1999, 2005). Moreover, using H_2O masers, distances to galaxies can be obtained without the use of standard candles (Miyoshi et al. 1995; Herrnstein et al. 1999; Argon et al. 2004, 2007; Brunthaler et al. 2005; Humphreys et al. 2008). Thus, finding new megamaser galaxies is of great interest.

If the unified scheme for AGNs is to be equally successful for objects of high as well as of low luminosity, there should exist a large number of type-2 QSOs whose optical spectra are dominated by narrow emission lines. Indeed, with the advent of new extended surveys such as the Sloan Digital Sky Survey (SDSS), many type-2 QSOs have recently been identified (Zakamska et al. 2003).

We conducted a search for water megamasers in 274 of the 291 SDSS type-2 AGNs (Zakamska et al. 2003) using the Robert C. Byrd Green Bank Telescope (GBT) and the Effelsberg 100 m radio telescope. With a redshift range of $0.3 < z < 0.83$, the sample covers significantly higher distances than most previous searches for H_2O megamasers ($z \ll 0.1$; Braatz et al. 1996, 2004; Tarchi et al. 2003; Kondratko et al. 2006a, 2006b; Braatz & Gugliucci 2008; Castangia et al. 2008) and is the first survey for water megamasers in objects with QSO luminosities (except for the study of Barvainis & Antonucci 2005 which is part of the larger survey presented here).

Such a search provides clues to whether the unified model can indeed be extended to QSOs or whether their powerful engines lead to a different scenario. Do the high QSO luminosities result in H_2O "gigamasers?" Or do they destroy the warm dense molecular gas needed to supply the water molecules? Are the molecular parts of the accretion disks much farther away from the nuclear engine, so that rotation velocities are smaller in spite of a potentially more massive nuclear engine than in Seyfert-2 galaxies? Finding megamasers in type-2 QSOs may provide insights into QSO molecular disks and tori and

[6] Current address: Department of Physics, University of California, Santa Barbara, CA 93106, USA.
[7] Any opinions, findings, conclusions, and recommendations expressed in this material are those of the author and do not necessarily reflect the views of the National Science Foundation.

enables us to independently determine their BH masses. Even more importantly, megamasers in type-2 QSOs may provide the unique possibility to directly measure their distances and thus verify the results from type 1a supernovae measurements on the existence and properties of the elusive dark energy (e.g., Barvainis & Antonucci 2005; Braatz et al. 2007; Reid et al. 2008).

We summarize the sample properties in Section 2, describe the observations in Section 3, present the results in Section 4, and discuss them in Section 5. After a brief summary (Section 6), we list a sample of 171 additional objects (radio galaxies, QSOs, and galaxies) in the Appendix. Throughout the paper, we assume a Hubble constant of $H_0 = 75$ km s^{-1} Mpc^{-1}. For the high-z objects, we additionally assume $\Omega_\Lambda = 0.73$ and $\Omega_M = 0.27$ (Wright 2006).

2. SAMPLE PROPERTIES

As already mentioned above, our sample consists of 274 type-2 AGNs ($0.3 < z < 0.83$) selected from the SDSS (Zakamska et al. 2003). Out of these, 122 objects have $L_{[O\,III]} > 3 \times 10^8 L_\odot$, and can thus be classified as type-2 QSOs (Zakamska et al. 2003). About 10% of the SDSS type-2 AGNs are radio loud (Zakamska et al. 2004), comparable to the AGN population as a whole. A few type-2 AGNs have soft X-ray counterparts (Zakamska et al. 2004). Spectropolarimetry was carried out for 12 type-2 QSOs and revealed polarization in all objects. Five objects show polarized broad lines expected in the framework of the unified model at the sensitivity achieved (Zakamska et al. 2005). Zakamska et al. (2006) studied the host galaxy properties for nine objects, finding that the majority (6/9) of the type-2 QSO host galaxies are ellipticals. All observations support the interpretation of the type-2 AGNs selected from the SDSS as being powerful obscured AGNs. Table 1 summarizes the sample properties.

3. OBSERVATIONS

All sources were measured in the 6_{16}–5_{23} line of H_2O (22.23508 GHz rest frequency). The observations were carried out during several runs at the GBT of the National Radio Astronomy Observatory (NRAO) in 2005 January and June as well as at the Effelsberg 100 m radio telescope of the Max-Planck-Institut für Radioastronomie (MPIR) in 2005 November and December. For details of observations, see Table 1.[8]

3.1. GBT

A total of 128 SDSS type-2 AGNs were observed with the GBT, limited to those that are within the available frequency coverage of 12–15.4 GHz ($0.44 < z < 0.85$). The observing mode utilized two feeds separated by 5′.5 on the sky, each with dual polarization. The system temperatures were typically 25 K. The source was placed alternately in each beam, with a position-switching interval of 2 minutes and was typically observed for 30 minutes total on-source time (possibly longer for objects with follow-ups). A total of 200 MHz bandwidth was covered with ∼0.5 km s^{-1} channels. Antenna pointing checks were made roughly every 2 hr, and typical pointing errors were less than 1/10 of a full width to half-power (FWHP) beamwidth of 48″ at 15 GHz. GBT flux calibration was done using standard antenna gain versus frequency curves. We estimate the calibration uncertainty to be ∼20%.

[8] Note that our velocity convention is the optical one, i.e., $v = cz$.

3.2. Effelsberg

A total of 150 SDSS type-2 AGNs were observed with the Effelsberg 100 m radio telescope.[9] The measurements were carried out with a dual polarization HEMT receiver providing system temperatures of ∼36–45 K (for the observed frequencies between ∼14.3 and 17.1 GHz) on a main beam brightness temperature scale. The observations were obtained in a position switching mode. Signals from individual on- and off-source positions were integrated for 3 minutes each, with the off-position offsets alternating between +900 and −900 arcsec in right ascension. The typical on-source integration time was ∼70 minutes (possibly longer for objects with follow-ups) with variations due to weather and elevation. An autocorrelator backend was used, split into eight bands of 40 MHz width and 512 channels, respectively, that were individually shifted in such a way that a total of ∼130–240 MHz was covered. Channel spacings are ∼1.5 km s^{-1}. The FWHP beamwidth was ∼40″. The pointing accuracy was better than 10″. Calibration was obtained by repeated measurements at different frequencies toward 3C 286, 3C 48, and NGC 7027, with flux densities taken from Ott et al. (1994), interpolated for the different observed frequencies using their Table 5. The calibration should be accurate to ∼20%.

4. RESULTS

All spectra were examined carefully by eye for both broad and narrow lines. In addition, we applied spectral binning using several bin sizes, especially if there was anything looking remotely like a signal.

4.1. The Gigamaser J0804+3607

As already reported in Barvainis & Antonucci (2005), water maser emission was detected from the type-2 QSO SDSS J080430.99+360718.1 (hereafter J0804+3607; $z = 0.66$). With $L_{H_2O} \simeq 21{,}000\ L_\odot$,[10] it is the intrinsically most powerful maser known.

4.2. Nondetections

While the detection of a water vapor maser in J0804+3607 shows that H_2O masers are indeed detectable at high redshift, and thus, that such a project is in principle feasible, no obvious maser emission was discovered in any of the remaining objects (Table 1). For some objects we see 2σ–3σ blips, which, however, do not meet the 5σ detection criterion. While they are most likely statistically insignificant, considering the effectively large number of trials implicit in the number of channels per spectrum, and the number of objects observed, follow-up observations are planned for verification.

5. DISCUSSION

Ideally, we would like to estimate the detection probabilities for our sample and compare them with the (non)detection rate.

In the local universe, water megamaser emission has been detected in about 10% of AGNs (Braatz et al. 2004). Simply extrapolating the percentage of megamasers detected in

[9] Note that a few objects were observed at both GBT and Effelsberg yielding a total number of 274 sources.

[10] Using $H_0 = 75$ km s^{-1} Mpc^{-1}, $\Omega_\Lambda = 0.73$, and $\Omega_M = 0.27$. Note that the value given by Barvainis & Antonucci (2005), $L_{H_2O} = 23{,}000\ L_\odot$, is higher due to a smaller value of H_0.

Table 1
Details of Observations: 274 SDSS Type-2 AGNs

Source	z	log $L_{[O\,III]}$	FIRST	ν	rms	v range	Channel Width	Telescope	Epoch
		($L_\odot$)	(mJy)	(MHz)	(mJy)	(km s^{-1})	(km s^{-1})		
(1)	(2)	(3)	(4)	(5)	(6)	(7)	(8)	(9)	(10)
080430.99+360718.1	0.658	8.83	76.96	13410.80	2.0	–2235,2235	0.5	GBT	0105
002531.46–104022.2	0.303	8.73	1.41	17064.53	9.1	–520,1150	1.4	Effelsberg	1105
002711.90+002231.8	0.437	7.92		15473.30	1.9	–1935,1935	0.5	GBT	0605
002827.78–004218.8	0.418	8.75		15680.59	6.0	–520,1320	1.5	Effelsberg	1105
002852.87–001433.6	0.310	8.43		16973.34	18.8	–1650,1600	1.4	Effelsberg	1205
004020.31–004033.5	0.568	8.25	97.70	14180.50	1.9	–2110,2110	0.5	GBT	0605
004412.87+003606.8	0.502	8.27		14803.60	2.1	–2025,2025	0.5	GBT	0105
005515.82–004648.6	0.345	8.15		16533.17	9.5	–1630,1710	1.4	Effelsberg	1205
005621.72+003235.8	0.484	9.45	8.60	14983.20	2.0	–2000,2000	0.5	GBT	0105
005733.95+001248.3	0.377	7.71		16147.48	8.6	–1680,1750	1.5	Effelsberg	1205

Notes. Column 1: source; boldface: the only object for which megamaser emission was detected (Barvainis & Antonucci 2005). Column 2: heliocentric redshift from Zakamska et al. (2003) as measured from the [O II] λ3727 emission line. Column 3: log ($L_{[OIII]}/L_\odot$) taken from Zakamska et al. (2003). A value of log ($L_{[OIII]}/L_\odot$) > 8.48 classifies the object as a type-2 QSO. Column 4: FIRST integrated fluxes at 20 cm in mJy taken from Zakamska et al. (2003), if the object is matched within 3″. There is no entry if the object was not detected [F_ν (20 cm) < 1 mJy]. "n/a" denotes those objects for which the field was not observed by the FIRST survey. Column 5: observed frequency ν in MHz. Column 6: rms flux density in mJy. Column 7: velocity range covered by observations in km s^{-1}. Column 8: channel width in km s^{-1}. Column 9: telescope at which the source was observed. Column 10: date of observations (mmyy).
(This table is available in its entirety in a machine-readable form in the online journal. A portion is shown here for guidance regarding its form and content.)

nearby Seyfert-2 galaxies to the more distant type-2 Seyferts and type-2 QSOs, leads to the expectation of finding at least ∼27 megamasers among the 274 SDSS type-2 AGNs. However, such a naive extrapolation does not take into account the megamaser luminosity function (LF), its evolution with redshift, the sensitivity of the survey, and intrinsic differences among the sources. We will discuss each of these issues in turn.

5.1. H_2O Maser LF

Henkel et al. (2005a) performed a statistical analysis of 53 H_2O maser galaxies beyond the Magellanic clouds. From the maser LF, i.e., the number density of objects with a given water maser luminosity per logarithmic interval in L_{H_2O}, they estimate that the number of detectable maser sources is almost independent of their intrinsic luminosity. The larger volume in which high-luminosity masers can be detected compensates the smaller source density. This implies that masers out to cosmological distances should be detectable with current telescopes, as long as the LF is not steepening at the very high end and if suitable candidates are available. Thus, Henkel et al. (2005a) conclude that most of the detectable luminous H_2O megamasers with $L_{H_2O} > 100 L_\odot$ have not yet been found.

We performed a similar analysis of the larger sample of masers known to date (78 sources; see Table 2) and derived a zeroth-order approximation of the LF of extragalactic water maser sources. We here briefly summarize the procedure adapted from Henkel et al. (2005a); for details and a discussion of limitations, we refer the reader to Henkel et al. (2005a). To estimate the water maser LF, the standard V/V_{max} method (Schmidt 1986) was used. We divided the 78 maser sources known to date (Table 2) in luminosity bins L_b of 0.5 dex ($b = 1, \ldots, 11$), covering a total range of $L_{H_2O}/L_\odot = 10^{-1}$–$(3 \times 10^4)$. The differential LF value was calculated for each luminosity bin according to

$$\Phi(L_b) = \frac{4\pi}{\Omega} \Sigma_{i=1}^{n(L_b)} (1/V_{max})_i,$$

where $n(L_b)$ is the number of galaxies with $L_b - 0.25 < \log(L_{H_2O}/L_\odot) \leqslant L_b + 0.25$ (centering on $\log(L_{H_2O}/L_\odot) = -0.75, -0.25, +0.25$, etc.). Following Henkel et al. (2005a), we set $\Omega = 2\pi$, approximating the sky coverage to be the entire northern sky, for the Seyfert sample. For J0804+3607, we assumed $\Omega = 0.64$ as the SDSS data release 1 from which the type-2 AGN sample of Zakamska et al. (2003) was taken covered ∼2100 deg^2. v_{max} is the maximum volume over which an individual galaxy can be detected depending on the detection limit of the survey and its maser luminosity (see also Section 5.2). We calculated the maser LF for three different detection limits: (a) 1 Jy km s^{-1}, (b) 0.2 Jy km s^{-1}, and (c) 0.06 Jy km s^{-1}. The first two cases are identical to the procedure in Henkel et al. (2005a); the latter case was added to include objects such as the gigamaser J0804+3607.[11] From the sample of 78 sources, IC 342 is excluded in all three cases due to its too low maser luminosity. In case (a), 32 masers fall below the chosen detection limit, and in case (b), 10 galaxies were omitted. In case (c), all 77 sources are included in the LF. The resulting LFs are shown in Figure 1.

The overall slope of the H_2O LF does not depend strongly on the chosen detection limit. Applying a linear fit to the three different LFs, we derive $\Phi \propto L_{H_2O}^{-1.4\pm0.1}$, comparable to Henkel et al. (2005a), but steeper than the LF for OH megamasers ($\Phi \propto L_{H_2O}^{-1.2}$; Darling & Giovanelli 2002). The main conclusions we can draw from this new version of the water maser LF are virtually identical to those by Henkel et al. (2005a). (1) The number of sources at the upper end of the LF decays rapidly, indicating that gigamasers are intrinsically rare or that the proper sources have not yet been found—so far most surveys were focused on nearby sources. In case (c), when including J0804+3607, the LF seems to raise again which is due to the much smaller area of sky covered in the survey presented here (see above). (2) There are only a few sources in the $L_{H_2O} =$ 0.1–10 $L_\odot$ bins. The associated slight minimum in the LF

[11] Note that for this distant object, we used the comoving volume as maximum volume.

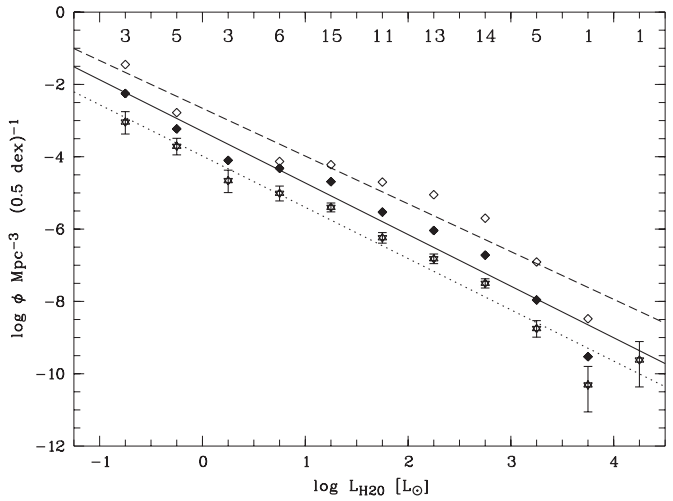

Figure 1. Luminosity function for water maser galaxies at $D \geqslant 100$ kpc (see Table 2). Plotted are the resulting LFs assuming three different sensitivity limits of the survey: 1 Jy km s^{-1} (open diamonds), 0.2 Jy km s^{-1} (filled diamonds), and 0.06 Jy km s^{-1} (open stars). The numbers on the top indicate the number of galaxies included in each luminosity bin for a sensitivity limit of 0.06 Jy km s^{-1} (open stars); corresponding error bars were calculated from Poisson statistics (Condon 1989). The lines indicate the best linear fit for a sensitivity limit of 1 Jy km s^{-1} (dashed line; $\Phi \propto L_{\rm H_2O}^{-1.3}$), 0.2 Jy km s^{-1} (solid line; $\Phi \propto L_{\rm H_2O}^{-1.4}$), and 0.06 Jy km s^{-1}, respectively (dotted line; $\Phi \propto L_{\rm H_2O}^{-1.4}$). See text for further details.

suggests that two different LFs are overlaid: one for masers in star-forming regions with low luminosities ($L_{\rm H_2O} < 0.1$–$10\ L_\odot$) and one for maser sources in AGNs with $L_{\rm H_2O} > 10\ L_\odot$.

However, note that an extrapolation of the local maser LF to higher redshifts is not straightforward. It would assume no cosmological evolution, but a strong evolution of AGN activity with redshift is known. Another cautionary note we want to add is that our survey is most sensitive to narrow-line masers and that we might be missing broad-line masers. Although we binned our data in various ways to emphasize potential broad-line masers and to make them more visible, a given amount of integrated flux density would then be spread over a larger amount of noise and baseline uncertainties would become more severe. Broad lines typically arise in jet masers such as Mrk 348 (Peck et al. 2003) and NGC 1052 (Claussen et al. 1998), one exception being TXS 2226-184 where a broad maser arises from a disk maser (Ball et al. 2005); for a discussion on jet masers see also Henkel et al. (2005b). As these broad-line masers are included in the LF of the known maser sources, we in principle introduce a systematic error when extrapolating the derived LF to our survey. However, since broad-line masers seem to be rare, we neglect this problem.

5.2. Sensitivity of the Survey

We can estimate the H_2O luminosities we would be able to detect depending on the sensitivity of our survey. Our sample lies at a redshift range of $0.3 < z < 0.83$, corresponding to luminosity distances of $D_L = 1460 - 4980$ Mpc.[12] The detectable H_2O luminosities depend on the sensitivity of the survey and the distance of the object (Henkel et al. 2005a). In general, it is

$$L = \frac{F_{\nu'}(\nu_0)}{1+z} \times 4\pi D_L^2,$$

with the specific flux $F_{\nu'}(\nu_0)$ in the observed frame. Then

$$\frac{L_{\rm H_2O}}{L_\odot} = \frac{10^{-23}\ S_{\rm peak}}{\rm Jy} \times \frac{\nu_{\rm rest}}{\rm c} \times \frac{\Delta v}{\rm km\,s^{-1}} \times \frac{1}{1+z} \times 4\pi \left(\frac{3.1\times10^{24}\ D_L}{\rm Mpc}\right)^2 \times \frac{1}{3.8\times10^{33}},$$

where $\nu_{\rm rest} = 22.23508$ GHz, and c is the speed of light in km s^{-1}. Thus,

$$\frac{L_{\rm H_2O}}{L_\odot} = \left[0.023 \times \frac{S_{\rm peak}}{\rm Jy} \times \frac{\Delta v}{\rm km\,s^{-1}}\right] \times \frac{1}{1+z} \times \left(\frac{D_L}{\rm Mpc}\right)^2;$$

(see also Solomon & Vanden Bout 2005). Assuming a characteristic line width of the dominant spectral feature of 20 km s^{-1}, a 5σ detection threshold of $5\times(7.6/4.5)$ mJy (with 7.6 mJy being the average rms of our observations for a 1 km s^{-1} channel) gives

$$\frac{L_{\rm H_2O}}{L_\odot} = 0.0039 \times \frac{1}{1+z} \times \left(\frac{D_L}{\rm Mpc}\right)^2.$$

Thus, given the distance of our sample, we can detect H_2O luminosities of $L_{\rm H_2O}$ 6400 − 52,900 $L_\odot$.

These H_2O luminosities are higher than the average luminosity found for megamasers in Seyfert-2 galaxies and LINERs. Among the 78 known H_2O maser galaxies, the typical cumulative H_2O luminosity range is 10–2000 $L_\odot$ for sources associated with AGNs, while most of the weaker masers appear to be related to star formation. However, in addition, there are two gigamasers known, TXS 2226–184 (Koekemoer et al. 1995) with $L_{\rm H_2O} =$ 6800 $L_\odot$ and J0804+3607 with $L_{\rm H_2O}$ 21,000 $L_\odot$. Thus, the distance of our sample allows us to detect gigamasers comparable to TXS 2226–184 and J0804+3607 only. The low detection rate may simply reflect that megamasers with H_2O luminosities above 6000 $L_\odot$ are intrinsically rare, an interpretation that is supported by the water maser LF (Section 5.1). However, there are other possibilities for the low detection rates that we discuss in the following.

5.3. Velocity Coverage

Our observations cover a frequency width of 130–240 MHz, corresponding to ∼1800–4000 km s^{-1}. This range should be large enough to cover any mismatch in redshift between the maser emission and the optical [O II] λ3727 emission. For J0804+3607, for example, the megamaser line is redshifted with respect to the [O II] line by 360 km s^{-1} (Barvainis & Antonucci 2005). However, we may not be able to detect superpositions of thousands of individual maser components with slightly differing velocities nor rapidly rotating tori with only the tangential parts showing strong (highly redshifted and blueshifted) maser emission (Henkel et al. 1998), if the emission covers a range of >2000 km s^{-1}.

5.4. Time Variability

Monitoring of megamaser sources has revealed variability on timescales of weeks with fluctuations of the order of 10% (e.g., Greenhill et al. 1997b) as well as on timescales of years with maser luminosities varying by factors of 3–10 (e.g., Falcke et al. 2000a; Gallimore et al. 2001; Tarchi et al. 2007). Such flaring masers can be explained by an increase in the X-ray luminosity

[12] Using $H_0 = 75$ km s^{-1} Mpc^{-1}, $\Omega_\lambda = 0.73$, and $\Omega_{\rm matter} = 0.27$.

Table 2
The 78 Galaxies at D 100 kpc with Known H_2O Masers

Source	R.A. (J2000)	Decl. (J2000)	v_{syst} (km s^{-1})	D (Mpc)	log L_{FIR} ($L_\odot$)	T_{dust} (K)	log L_{H_2O} ($L_\odot$)	Morph.	Type	Ref.
(1)	(2)	(3)	(4)	(5)	(6)	(7)	(8)	(9)	(10)	(11)
NGC 23	00 09 53.6	+25 55 23	4566	60.9	11.1	45	2.2	SB(s)a	L,LIRG,H II	1
IC 10	00 20 27.0	+59 17 29	–350	1.2	8.2	40	–0.8	dIRR		2,3
	00 20 17.9	+59 18 31					–1.7			4
NGC 235A	00 42 52.8	–23 32 28	6519	86.9	11.4	44	2.0	S0 pec	Sy1	5
NGC 253	00 47 33.1	–25 17 17	240	3.0	10.3	52	–0.8	SAB(s)c	Sy2,SB,H II	6,7
	00 47 33.6	–25 17 14					–1.7			7
NGC 262 (Mrk 348)	00 48 47.1	+31 57 25	4505	62.0	10.4	54	2.6	SA(s)0/a:	Sy2	8,9
ESO 013–G012	01 07 00.9	–80 18 24	5045	67.0	10.7	32	2.7	Sa		10
NGC 449 (Mrk 1)	01 16 07.2	+33 05 22	4780	64.0	10.7	55	1.7	(R')S?	Sy2	11
NGC 520	01 24 34.9	+03 47 30	2281	30.4	10.9	48	0.3	Pec	SB,H II	12
NGC 598 (M 33)[a]	01 33 16.5	+30 52 53	–180	0.7	9.0	36	–0.5	SA(s)cd	H II	13,14,15,16
	01 33 28.3	+30 31 43					–1.5			15,16
	01 34 00.2	+30 40 47					–2			16,17
NGC 591 (Mrk 1157)	01 33 31.2	+35 40 06	4555	61.0	10.5	46	1.4	(R')SB0/a	Sy2	18
NGC 613	01 34 18.2	–29 25 07	1481	17.9	10.4	38	1.3	SB(rs)bc	Sy,H II	5,12
IC 0184	01 59 51.2	–06 50 25	5287	70.5	9.9[b]	40[b]	1.4	SB(r)a:	Sy2,H II	5
NGC 1052	02 41 04.8	–08 15 21	1470	17.0	9.2	54	2.1	E4	Sy2,L	11,20
NGC 1068	02 42 40.7	–00 00 48	1135	14.5	11.2	54	2.2	(R)SA(rs)b	Sy1,Sy2	21,22
NGC 1106	02 50 40.5	+41 40 17	4337	57.8	10.3	49	0.9	SA0+	Sy2	1
Mrk 1066	02 59 58.6	+36 49 14	3600	48.0	10.9	55	1.5	(R)SB(s)0+	Sy2	18,23
NGC 1386	03 36 46.4	–36 00 02	870	17.0	9.8	46	2.1	SB(s)0+	Sy2	24
IRAS 03355+0104	03 38 10.4	+01 14 18	11926	159.0	11.2	36	2.7[c]	S0/a	Sy2	19
IC 342[d]	03 46 46.3	+68 05 46	40	2.0	9.0	49	–2.0	SAB(rs)cd	Sy2,H II	25
UGC 3193	04 52 52.7	+03 03 24	4454	59.4	10.6	43	2.4	SB(rs)ab:		1
UGC 3255	05 09 50.2	+07 29 00	5675	75.0	10.6	40	1.2	SBb?	Sy2	18
Mrk 3	06 15 36.3	+71 02 15	4010	54.0	10.7	69	1.0	S0:	Sy2	18
NGC 2146	06 18 36.6	+78 21 28	900	14.5	10.9	53	0.0[e]	SB(s)ab pec	H II	26
	06 18 38.6	+78 21 24					0.0[e]			26
VII Zw 073	06 30 25.6	+63 40 41	11899	158.7	11.2	51	2.2		Sy2	5
NGC 2273	06 50 08.7	+60 50 45	1840	24.5	10.1	47	0.8	SB(r)a	Sy2	27
UGC 3789	07 19 30.9	+59 21 18	3325	44.3	10.2	42	2.5	(R)SA(r)ab		1
Mrk 78	07 42 41.7	+65 10 37	11195	150.0	11.0	60	1.5	SB	Sy2	18
Mrk 1210	08 04 05.8	+05 06 50	4045	54.0	10.5	75	1.9	Sa	Sy1,Sy2	11
SDSS J0804+3607	08 04 31.0	+36 07 18	$z = 0.66$	3749.7[f]	···	···	4.3[f]		QSO2	28
2MASX J0836+3327	08 36 22.8	+33 27 39	14810	197.5	···	···	3.4[c]		Sy2	19
NGC 2639	08 43 38.1	+50 12 20	3335	44.0	10.4	34	1.4	(R)SA(r)a:?	Sy1.9	11,29
NGC 2782	09 14 05.1	+40 06 49	2560	34.0	10.5	47	1.1	SAB(rs)a	Sy1,SB	18
NGC 2824 (Mrk 394)	09 19 02.2	+26 16 12	2760	37.0	9.9	47	2.7	S0	Sy?	30
SBS 0927+493	09 31 06.7	+49 04 47	10167	135.6	11.2	52	2.7[c]		L[g]	19
UGC 5101	09 35 51.6	+61 21 11	11809	157.5	12.0	46	3.2	S?	Sy1.5,L,LIRG	27
NGC 2960 (Mrk 1419)	09 40 36.4	+03 34 37	4930	66.0	10.4	40	2.6	Sa?	L[g]	31
NGC 2979	09 43 08.5	–10 23 01	2720	36.0	10.0	40	2.1	(R')SA(r)a?	Sy2	30
NGC 2989	09 45 25.8	–18 22 36	4146	55.3	10.5	38	1.6	SAB(s)bc:	H II	1
NGC 3034 (M 82)	09 55 52.2	+69 40 47	200	3.7	10.6	65	0.0	I0	SB,H II	21,32
NGC 3079	10 01 57.8	+55 40 47	1120	15.5	10.6	42	2.7	SB(s)c	Sy2,L	33,34,35
IC 2560	10 16 18.7	–33 33 50	2925	35.0	10.2	47	2.0	(R')SB(r)bc	Sy2,H II?	24,36
Mrk 34	10 34 08.6	+60 01 52	15140	205.0	11.3	56	3.0	Spiral	Sy2	23
NGC 3359	10 46 36.8	+63 13 25	1014	13.5	9.6	34	–0.2	SB(rs)c	H II	1
NGC 3393	10 48 23.4	–25 09 43	3750	50.0	10.4	46	2.6	(R')SB(s)ab	Sy2	5,27
NGC 3556	11 11 31.2	+55 40 25	700	12.0	10.2	38	0.0	SB(s)cd	H II	23
Arp 299 (Mrk 171)	11 28 32.2	+58 33 44	3120	42.0	11.7	61	2.1	IBm/SBm		23
NGC 3735	11 35 57.3	+70 32 09	2695	36.0	10.6	38	1.3	SAc	Sy2	37
NGC 4051	12 03 09.6	+44 31 53	730	10.0	9.6	38	0.3	SAB(rs)bc	Sy1.5	38
NGC 4151	12 10 32.6	+39 24 21	1000	13.5	9.8	52	–0.2	(R')SAB(rs)ab:	Sy1.5	18
NGC 4258	12 18 57.5	+47 18 14	450	7.2	9.9	33	1.9	SAB(s)bc	Sy1.9,L	21,39
NGC 4293	12 21 12.9	+18 22 57	890	17	9.7	40	0.7	(R)SB(s)0/a	L	5
NGC 4388	12 25 46.7	+12 39 44	2520	34.0	10.7	47	1.1	SA(s)b:	Sy2	18
NGC 4527	12 34 08.5	+02 39 14	1736	23.2	10.8	39	0.6	SAB(s)bc	L,H II	1
ESO 269–G012	12 56 40.7	–46 55 31	4950	66.0	10.5	41	3.0	S0	Sy2	30
NGC 4922	13 01 25.2	+29 18 50	7080	95.0	11.2	61	2.3	I0/p	Sy2,L	18
NGC 4945	13 05 27.5	–49 28 06	560	4.0	10.3	45	1.7	SB(s)cd	Sy2	40,41
NGC 5194 (M 51a)	13 29 52.7	+47 11 43	450	10.0	10.3	33	–0.2	SA(s)bc pec	Sy2,H II	6,42
NGC 5256 (Mrk 266)	13 38 17.2	+48 16 32	8365	112.0	11.5	46	1.5	Pec	Sy2,LIRG,SB	18
NGC 5347	13 53 17.8	+33 29 27	2335	31.0	9.9	44	1.5	(R')SB(rs)ab	Sy2	24

Table 2
(Continued)

Source	R.A. (J2000)	Decl. (J2000)	v_{syst} (km s^{-1})	D (Mpc)	log L_{FIR} ($L_\odot$)	T_{dust} (K)	log L_{H_2O} ($L_\odot$)	Morph.	Type	Ref.
(1)	(2)	(3)	(4)	(5)	(6)	(7)	(8)	(9)	(10)	(11)
NGC 5495	14 12 23.3	–27 06 29	6589	87.8	10.8	39	2.3	(R')SA(rs)b	Sy2,H II?	5
Circinus	14 13 09.3	–65 20 21	450	4.0	10.1	54	1.3	SA(s)b:	Sy2	43,44
NGC 5506 (Mrk 1376)	14 13 14.8	–03 12 27	1850	25.0	10.3	59	1.7	SA pec	Sy1.9	11
NGC 5643	14 32 40.7	–44 10 28	1200	16.0	10.3	39	1.4	SAB(rs)c	Sy2	30
NGC 5728	14 42 23.9	–17 15 11	2795	37.0	10.6	45	1.9	(R_1)SAB(r)a	Sy2,H II	18
UGC 9618B	14 57 00.7	+24 37 03	10094	134.6	11.7	39	3.2[c]	(Sb)	L,H II	19
NGC 5793	14 59 24.7	–16 41 36	3490	47.0	10.6	47	2.0	Sb:	Sy2	45,46
NGC 6240	16 52 58.1	+02 23 50	7340	98.0	11.8	58	1.6	I0: pec	Sy2,L	47,48,49,50
NGC 6264	16 57 16.1	+27 50 59	10177	135.7	...	...	3.1[c]	Sb	Sy2	19
NGC 6323	17 13 18.0	+43 46 56	7790	104.0	10.3[h]	35[h]	2.7	Sab	Sy2	18
NGC 6300	17 17 00.3	–62 49 15	1110	15.0	10.2	36	0.5	SB(rs)b	Sy2	30
ESO 103–G035	18 38 20.3	–65 25 42	3985	53.0	10.5	121	2.6	SA0	Sy1,Sy2	24
IRAS F19370–0131	19 39 38.9	–01 24 33	6000	80.0	10.7	59	2.2	Sb	Sy2,H II	30
3C 403	19 52 15.8	+02 30 24	17690	235.0	11.3[i]	... [i]	3.3	S0	NLRG	51
NGC 6926	20 31 38.7	–80 49 58	5970	80.0	11.2	39	2.7	SB(s)bc pec	Sy2,H II	30
AM 2158–380b	22 01 17.1	–37 46 24	9661	128.8	10.4[h]	49[h]	2.7	Sa	Sy2,RG	5
TXS 2226–184	22 29 12.5	–18 10 47	7495	100.0	...	...	3.8	S?[j]	L	52
NGC 7479	23 04 56.7	+12 19 22	2381	31.75	10.7	42	1.2	SB(s)c	Sy2,L	1
IC 1481	23 19 25.1	+05 54 21	6120	82.0	10.6	65	2.5	S?	L	24

Notes. Column (1): source. Columns (2,3): R.A. and Decl. (J2000). Column (4): systemic velocity $v = cz$ (km s^{-1}) taken from NED. Column (5): distance (Mpc), using $H_0 = 75$ km s^{-1} Mpc^{-1}. For the 53 of the 78 masers that were included in Henkel et al. (2005a), we adapt the distances from their Table 4. For a few objects, we take distances from the references listed in Column (11). Columns (6, 7): far-infrared (FIR) luminosity log ($L_{FIR}/L_\odot$) and dust temperature T_{dust} in K. For the determination of L_{FIR} and T_{dust} (60/100 μm color temperatures), see Wouterloot & Walmsley (1986). The *IRAS* fluxes were taken from Fullmer & Lonsdale (1989) and, for a few sources (NGC 262, NGC 598, IC 0184, NGC 4151, NGC 4258, *IRAS* F19370–0131, NGC 6323, 3C 403, and AM 2158–380b), from NED. Column (8): log ($L_{H_2O}/L_\odot$), using $H_0 = 75$ km s^{-1} Mpc^{-1}. Column (9): host galaxy morphology type taken from NED. Column (10): activity type taken from NED (Sy = Seyfert, L = LINER, LIRG = luminous-infrared galaxy, SB = starburst, NLRG = narrow-line radio galaxy, RG = radio galaxy). Column (11): References: [1] Braatz & Gugliucci (2008); [2] Becker et al. (1993); [3] Argon et al. (1994); [4] Henkel et al. (1986); [5] Kondratko et al. (2006b); [6] Ho et al. (1987); [7] Henkel et al. (2004); [8] Falcke et al. (2000a); [9] Peck et al. (2003); [10] Greenhill et al. (2002); [11] Braatz et al. (1994); [12] Castangia et al. (2008); [13] Churchwell et al. (1977); [14] Greenhill et al. (1993); [15] Huchtmeier et al. (1978); [16] Brunthaler et al. (2006); [17] Huchtmeier et al. (1988); [18] Braatz et al. (2004); [19] Kondratko et al. (2006a); [20] Claussen et al. (1998); [21] Claussen et al. (1984); [22] Gallimore et al. (2001); [23] Henkel et al. (2005a); [24] Braatz et al. (1996); [25] Tarchi et al. (2002a); [26] Tarchi et al. (2002b); [27] Zhang et al. (2006); [28] Barvainis & Antonucci (2005); [29] Wilson et al. (1995); [30] Greenhill et al. (2003a); [31] Henkel et al. (2002); [32] Baudry & Brouillet (1996); [33] Henkel et al. (1984); [34] Haschik & Baan (1985); [35] Trotter et al. (1998); [36] Ishihara et al. (2001); [37] Greenhill et al. (1997a); [38] Hagiwara et al. (2003b); [39] Herrnstein et al. (1999); [40] Dos Santos & Lépine (1979); [41] Greenhill et al. (1997b); [42] Hagiwara et al. (2001b); [43] Gardner & Whiteoak (1982); [44] Greenhill et al. (2003b); [45] Hagiwara et al. (1997); [46] Hagiwara et al. (2001a); [47] Hagiwara et al. (2002); [48] Nakai et al. (2002); [49] Braatz et al. (2003); [50] Hagiwara et al. (2003a); [51] Tarchi et al. (2003); [52] Koekemoer et al. (1995).

[a] While the detection of two more masers has been claimed by Huchtmeier et al. (1978, 1988), we list only the three masers confirmed by Brunthaler et al. (2006).

[b] L_{FIR} and T_{dust} are lower limits as there are no *IRAS* flux measurements at 12 and 25μm.

[c] Estimated from Figure 1 of Kondratko et al. (2006a) using $L_{H_2O}/L_\odot = 0.023\ S_{total}/(\mathrm{Jy\ km\ s^{-1}}) \times D^2/\mathrm{Mpc}$ with $S_{total} = \sum (1.06\ S_{peak} \times \mathrm{FWHM})$ (summed over the different components).

[d] The maser luminosity refers to a brief flaring episode.

[e] We assume log $L_{H_2O}/L_\odot = 0.9$ as total integrated single-dish flux density when including NGC 2146 in Figures 1, 2, and 3.

[f] Using $H_0 = 75$ km s^{-1} Mpc^{-1}, $\Omega_\Lambda = 0.73$, and $\Omega_M = 0.27$.

[g] Note that NED gives "Sy3" as classification, which corresponds to a LINER (Veron-Cetty & Veron 1996).

[h] There is no *IRAS* flux measurement at 12 μm.

[i] There is no *IRAS* flux measurement at 100 μm.

[j] Note that while NED lists "E/S0" as morphological classification of the host galaxy according to Koekemoer et al. (1995), Falcke et al. (2000b) favor a classification as a highly inclined spiral galaxy. We use the latter in our statistics in Section 5.

of the AGN (Neufeld 2000), if the maser emission is powered by the X-ray radiation from the AGN.

We cannot exclude that at least some of the sources for which we did not detect megamaser emission were in a low stage of maser activity and might be detected at a later flaring stage.

5.5. Intrinsic Differences

So far, we did not take into account that, when comparing the low-luminous AGNs such as Seyfert-2 galaxies and LINERs with the high-luminous AGNs such as the type-2 QSOs in our sample, we may be comparing apples and oranges. Intrinsic differences between the different samples complicate estimating detection probabilities.

5.5.1. The Nature of Megamaser Galaxies

So far, ~1500 galaxies have been searched for H_2O maser emission, resulting in the detection of 78 maser galaxies (Table 2). For 73 of the 78 known H_2O maser galaxies, the

activity type has been determined (NED;[13] see Table 2). The vast majority are classified as Seyferts (78%), out of which Sy2s (including Sy1.9) are the dominant type (88%) and Sy1s are rare (3%), the rest being classified simply as Sy, or Sy1.5. The second largest activity type among the extragalactic water maser sources are LINERs, making up 11% of the sample. In addition, 7% are H II regions, 3% starburst (SB) galaxies and 1% narrow-line radio galaxies (NLRGs).[14]

Objects with activity type of H II or SB have generally lower maser luminosities and fall in the kilomaser range ($L_{H_2O} < 10\,L_\odot$). When including only maser sources with $L_{H_2O} \geqslant 10 L_\odot$, the activity type has been determined for 57 sources in total. Out of these, 86% are Seyferts (82% are Sy2s; 4% are Sy1s, namely NGC 235A and NGC 2782), 10% are LINERs, and only 2% are H II regions (namely NGC 2989).

Using the higher number of extragalactic water maser sources known to date, our statistic thus confirms earlier studies that water megamaser sources are associated with AGNs of primarily Seyfert-2 or LINER type (Braatz et al. 1997, 2004). This in turn strengthens the general expectation to find megamasers also in type-2 QSOs.

Interpreting this finding in the framework of the unified models of AGNs, where an optically thick obscuring dust torus is envisioned to encircle the accretion disk and type-1 AGNs are seen pole-on, while type-2 AGNs are seen edge-on (Antonucci 1993), suggests that the megamaser activity is related to the large column densities of molecular gas along the line of sight in the torus. However, even if such an interpretation holds, the question remains why not all type-2 AGNs are megamasers. What are the necessary ingredients for the occurrence of these powerful masers?

Braatz et al. (1997) addressed this question by a statistical comparison of the physical, morphological, and spectroscopic properties of the known megamaser galaxies with those of nonmegamaser galaxies.[15] They compared the AGN class, the host galaxy type and inclination, the mid-infrared (MIR) and FIR properties, the radio fluxes and luminosities, the [O III] fluxes and luminosities, and the X-ray properties of the 16 megamasers known at that time with those of ∼340 nonmegamaser galaxies. Apart from their main conclusion that H_2O emission is only detected in Seyfert-2 galaxies and LINERs but not in Seyfert-1 galaxies (a conclusion that still holds for the larger sample of megamasers known today; see above), Braatz et al. (1997) found that H_2O emission is preferentially detected in sources that, when compared to the nonmegamaser galaxies in their sample, are "apparently brighter at MIR and FIR and centimeter radio wavelengths." However, this result may at least in part result from the fact that the megamaser galaxies are nearer than the nonmegamaser galaxies. Braatz et al. (1997) also find that H_2O emission is preferentially detected in sources with high X-ray-absorbing columns of gas—a result that is still discussed controversially. While Zhang et al. (2006) concluded that H_2O megamasers have similar X-ray-absorbing column densities as other Seyfert-2 galaxies, Greenhill et al. (2008) find a correlation between maser emission and high X-ray-obscuring columns.

[13] Note that NED classifications such as morphological types and activity classes are inhomogeneous.

[14] Note that we counted the "more energetic" activity type, e.g., an object with activity types "Sy2, SB, H II" (Table 2, Column 10), was counted as Sy2, an object with "L, LIRG, H II," was counted as LINER, etc.

[15] Here and in the following, we denote as "nonmegamaser galaxies" those galaxies that have been observed at 22 GHz, but for which no megamaser emission was detected.

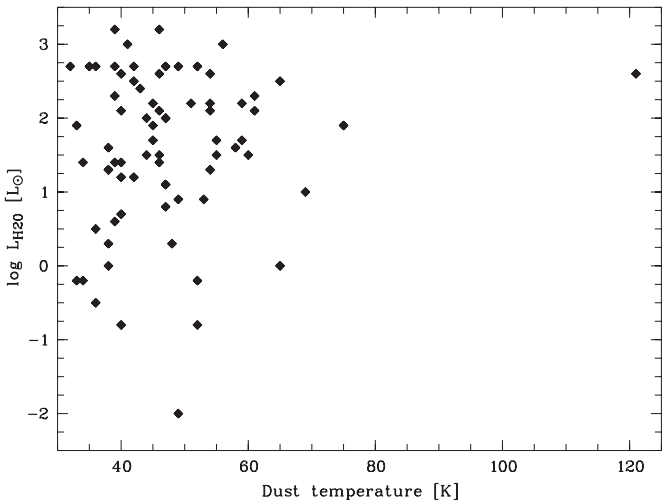

Figure 2. Water maser luminosities vs. dust temperatures of H_2O detected galaxies (see Table 2; excluding those objects for which we do not have dust temperatures, leaving us with 73 objects total).

The requirement for velocity coherence may play an important role for the (non)occurrence of megamasers. For NGC 4258, for example, the scattered light requires a thick-obscuring disk (in terms of its optical shadowing properties) but the masers reside in a thin disk (Wilkes et al. 1995; Barth et al. 1999; Humphreys et al. 2008). Enough velocity coherence (and gas column density) is perhaps achieved most often in the midplane. Thus, the solid angle into which the water maser emission is beamed is small, much smaller than that of the torus. With such a small angle, the likelihood to observe a maser line depending on the viewing angle is small as well.

However, now, over 10 years after the study of Braatz et al. (1997), the number of known megamaser galaxies has more than quadrupled. But there is no comparable study addressing the IR properties of megamasers, their host galaxies and their radio and optical properties. Such a study might reveal the necessary ingredients for the occurrence of megamasers in AGNs. This in turn would greatly facilitate the preselection of promising candidates for megamaser emission among type-2 QSOs. However, such a detailed comparison is beyond the scope of this paper.

5.5.2. FIR Luminosities and Dust Temperatures

Here, we derive the FIR luminosities and dust temperatures from *IRAS* fluxes (Fullmer & Lonsdale 1989) using the procedure of Wouterloot & Walmsley (1986). Some caution is required because these *IRAS* measurements are affected by the ratio of the contribution of nuclear light to host light which depends on nuclear FIR luminosity, nature of the host, and metric aperture size (and thus distance). Table 2 gives FIR luminosities and dust temperatures for the sample of known maser sources. The latter are all well above 30 K and thus rather large, as already noted by Henkel et al. (1986, 2005a); Braatz et al. (1997).[16] There is no obvious relation between dust temperatures and L_{H_2O} (Figure 2). In Figure 3, we show the FIR luminosity versus water maser luminosity. There seems to be a correlation between FIR luminosity and water maser luminosities in the sense that higher FIR luminosity lead to higher

[16] Note that the dust temperatures were calculated from the 60/100μm flux ratio. Cooler dust might be dominant in these galaxies but does not radiate at these wavelengths.

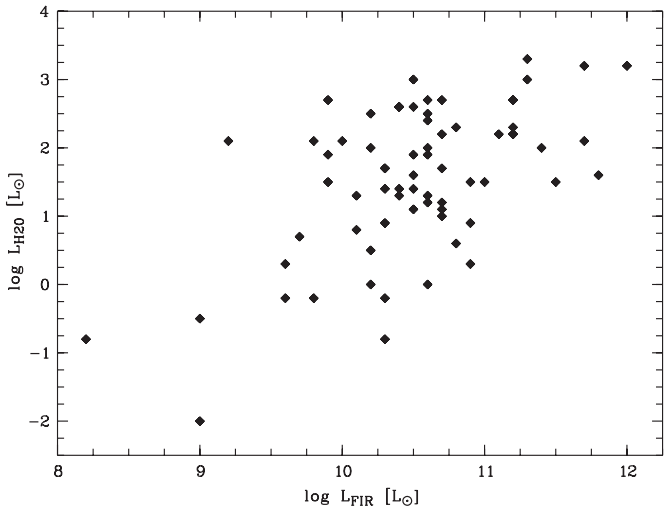

Figure 3. *IRAS* point source FIR luminosity vs. total H_2O luminosity of H_2O detected galaxies (see Table 2; excluding those objects for which we do not have FIR luminosities as well as those for which we only have lower limits, leaving us with 71 objects total).

Table 3
SDSS Type-2 AGNs with *IRAS* Flux Measurements

Source	z	D (Mpc)	log L_{FIR} ($L_\odot$)	T_{dust} (K)
(1)	(2)	(3)	(4)	(5)
022606.86–001656.0	0.407	2087.5	13.3	37
024919.01–000722.5	0.579	3193.5	13.7	37
031319.96+003715.6	0.395	2014.6	13.3	38
032240.60+001626.0	0.344	1711.3	13.1	35
075238.68+390304.9	0.654	3707.8	13.8	37
110709.36+511328.6	0.441	2297.4	13.5	32
123453.10+640510.2	0.594	3294.9	13.9	37
172603.09+602115.7	0.333	1647.4	13.1	35

Notes. Column 1: source. Column 2: heliocentric redshift from Zakamska et al. (2003) as measured from the [O II] λ3727 emission line. Column 3: distance (Mpc), using $H_0 = 75$ km s^{-1} Mpc^{-1}, $\Omega_\Lambda = 0.73$, and $\Omega_M = 0.27$. Columns 4 and 5: FIR luminosity log ($L_{FIR}/L_\odot$) and dust temperature T_{dust} in K (see also Table 2 and text for details).

water maser luminosities. However, we do not claim that the maser luminosity versus FIR luminosity plot shows an intimate physical connection between both properties. Instead, Figure 3 mainly shows the range of FIR and H_2O luminosities covered by the known megamaser sources.

Unfortunately, for our sample of 274 SDSS type-2 AGNs, *IRAS* fluxes are only available for eight objects (see Table 3). Keeping in mind the small number statistics, it is interesting to note that the average dust temperature for these eight objects, $T_{dust,ave}$ 36 ± 1 K, is by ∼12 K lower than the one for the known maser galaxies ($T_{dust,ave}$ 48 ± 2 K). At the same time, the type-2 AGNs of the SDSS sample all have very high FIR luminosities (log($L_{FIR}/L_\odot$) 13.5 ± 0.1) compared to the maser sources (log($L_{FIR}/L_\odot$) 10.5 ± 0.1), which are of course a lot closer.

5.5.3. BH Mass and Accretion Disk

One difference between the high-z type-2 AGNs in our sample and the local Seyfert-2 galaxies and LINERs in which megamasers have been found is the mass of the central engine. For Seyfert galaxies, BH masses range between ∼10^6 $M_\odot$ and a few 10^7 $M_\odot$ (e.g., Greenhill et al. 1997b; Herrnstein et al. 1999; Henkel et al. 2002), while masses in QSOs can reach 10^9 $M_\odot$ or more (e.g., Labita et al. 2006; Vestergaard et al. 2008). Tarchi et al. (2007) suggest that clouds in a disk with large rotational velocity and small galactocentric radius like NGC 4258 might not be stable in the vicinity of such a large BH mass.

5.5.4. Dust Torus and X-ray Luminosity

Barvainis & Antonucci (2005) have argued that extremely powerful masers might be expected from high-luminosity QSOs. With every square parsec of area illuminated by the primary AGN X-ray emission, a luminosity of ∼100 $L_\odot$ is produced (Neufeld et al. 1994). The area of the torus illuminated by the AGN increases with the optical/UV continuum luminosity as the dust sublimation radius scales as $L_{opt/UV}^{1/2}$. Indeed, a scenario in which the high QSO luminosities result in gigamasers is consistent with the detection of J0804+3607, by far the most powerful maser known today. If r_{sub} increases with optical/UV luminosity, also the molecular parts giving rise to the maser emission are expected to arise further away from the nuclear engine. Such a prediction can be tested observationally. We would expect to observe rotation velocities that are smaller than in Seyfert-2 galaxies, despite a potentially more massive BH.

However, these considerations do not take into account that the dust-covering factor may be decreasing with optical luminosity (Simpson 2005). In addition, the water maser luminosity is expected to grow more slowly than optical luminosity, since $L_{X\text{-ray}}/L_{opt}$ seems to be a declining function with increasing luminosity (Vignali et al. 2003). These two effects may cause megamasers to be intrinsically rare among type-2 QSOs.

5.5.5. Host Galaxy

One known difference between QSOs and Seyfert galaxies is their host galaxies: while the majority of Seyfert galaxies reside in spiral-like galaxies, QSOs are found predominantly in early-type galaxies (e.g., Disney et al. 1995; Bahcall et al. 1997; McLure et al. 1999; Floyd et al. 2004).

Among the 78 known H_2O maser galaxies, the host galaxy properties have been determined for 74 objects (NED;[17] see Table 2). The majority of known megamasers resides in spiral galaxies (∼84%), of which more than half were classified as barred or at least weakly barred galaxies (53%). Seven percent of the host galaxies were classified as SO, and only 1% as elliptical galaxies, the rest as irregular or peculiar galaxies (∼8%). It is remarkable that only one galaxy, namely NGC 1052, has an elliptical morphology. Also, the search for megamaser emission from early-type galaxies with FRI radio morphology leads to no detection (Henkel et al. 1998).

Does this imply that spiral galaxies somehow favor the presence of megamaser activity? Elliptical galaxies may simply lack the molecular gas necessary for the occurrence of H_2O masers. With respect to the nuclear activity, one important difference between spiral galaxies and early-type galaxies seems to be the fueling mechanism. While there is now convincing evidence that most if not all QSOs are triggered by mergers (e.g., Hutchings et al. 1994; Canalizo & Stockton 2001; Guyon et al. 2006; Canalizo et al. 2007; Bennert et al. 2008; Urrutia et al. 2008), their low-luminous cousins, Seyfert galaxies, do

[17] As noted above, the morphological types given by NED are inhomogeneous.

Table 4
Details of Observations: Radio Galaxies

Source	R.A.	Decl.	z	ν	rms	v range	Channel Width	Telescope	Epoch
	(J2000)			(MHz)	(mJy)	(km s^{-1})	(km s^{-1})		
(1)	(2)	(3)	(4)	(5)	(6)	(7)	(8)	(9)	(10)
RC 0008+172	00 11 07.5	+17 29 48	1.390	9303.35	2.8	–820,805	1.5	Arecibo	1003
3C 005	00 13 10.5	+00 51 32	0.606	13858.80	1.4	–2160,2160	0.5	GBT	0605
PMN J0018+0940	00 18 55.2	+09 40 07	1.586	8598.22	2.2	–870,870	1.7	Arecibo	1003
B2 0026+34	00 29 14.2	+34 56 32	0.517	14657.30	2.1	–2045,2045	0.5	GBT	0605
4C +45.02	00 30 52.1	+45 21 48	0.365	16289.00	12.5	–1670,1720	1.4	Effelsberg	1205
3C 016	00 37 44.6	+13 19 55	0.405	15826.00	11.7	–1720,1780	1.5	Effelsberg	1205
PKS 0037–009	00 40 20.3	–00 40 33	0.568	14180.50	2.0	–2110,2110	0.5	GBT	0605
3C 19	00 40 55.0	+33 10 08	0.482	15003.40	1.9	–1995,1995	0.5	GBT	0605
MRC 0044+107	00 46 41.4	+11 02 53	1.813	7904.37	0.7	–950,950	1.8	Arecibo	0904
MG3 J005335+2045	00 53 37.9	+20 46 03	1.297	9680.02	3.3	–770,770	1.5	Arecibo	1003

Notes. Column 1: source. Columns 2 and 3: R.A. and Decl. (J2000) taken from NED. Column 4: heliocentric redshift z taken from NED. Column 5: observed frequency ν in MHz. Column 6: rms flux density in mJy. Column 7: velocity range covered by observations in km s^{-1}. Column 8: channel width in km s^{-1}. Column 9: telescope at which the source was observed. Column 10: date of observations (mmyy).
(This table is available in its entirety in a machine-readable form in the online journal. A portion is shown here for guidance regarding its form and content.)

Table 5
Details of Observations: Miscellaneous Sources

Source	Classification	R.A.	Decl.	z	ν	rms	v range	Channel Width	Telescope	Epoch
		(J2000)			(MHz)	(mJy)	(km s^{-1})	(km s^{-1})		
(1)	(2)	(3)	(4)	(5)	(6)	(7)	(8)	(9)	(10)	(11)
081404.54+060238.3	QSO	08 14 04.5	+06 02 38	0.561	14235.00	2.3	–2105,2105	0.5	GBT	0605
082110.76+031758.4	QSO	08 21 10.8	+03 17 58	0.451	15324.00	3.3	–1955,1955	0.5	GBT	0605
083134.21+290239.5	G	08 31 34.2	+29 02 40	0.568	14180.50	1.5	–2110,2110	0.5	GBT	0605
091345.49+405628.2	G	09 13 45.5	+40 56 28	0.442	15430.30	2.2	–1940,1940	0.5	GBT	0605
092344.07+081051.2	QSO	09 23 44.1	+08 10 51	0.415	15703.00	12.7	–1730,1780	1.5	Effelsberg	1205
093737.11+370535.4	G	09 37 37.1	+37 05 35	0.449	15334.60	2.2	–1955,1955	0.5	GBT	0605
095005.83+481338.6	G	09 50 05.8	+48 13 39	0.375	16171.00	11.9	–1680,1730	1.4	Effelsberg	1205
095019.90+051140.9	G	09 50 19.9	+05 11 41	0.523	14590.00	2.0	–2055,2055	0.5	GBT	0605
100258.68+050812.0	G	10 02 58.7	+05 08 12	0.512	14705.70	2.0	–2035,2035	0.5	GBT	0605
101401.59+431543.4	G	10 14 01.6	+43 15 43	0.511	14715.50	2.0	–2035,2035	0.5	GBT	0605

Notes. Column 1: source. Column 2: classification as Galaxy (G) or QSO, taken from NED. Columns 3 and 4: R.A. and Decl. (J2000) taken from NED. Column 5: heliocentric redshift z taken from NED. Column 6: observed frequency ν in MHz. Column 7: rms flux density in mJy. Column 8: velocity range covered by observations in km s^{-1}. Column 9: channel width in km s^{-1}. Column 10: telescope at which the source was observed. Column 11: date of observations (mmyy).
(This table is available in its entirety in a machine-readable form in the online journal. A portion is shown here for guidance regarding its form and content.)

not show unusually high rates of interaction (e.g., Malkan et al. 1998). For Seyferts, the gas necessary for the fueling of the AGN may simply be provided by their spiral host galaxies and funneled into the very center through bar instabilities (Combes 2006).[18] Bars may also play an important role for the obscuration of the central AGN (Maiolino et al. 1999). Is the fueling via bar instabilities a more stable mechanisms ensuring the existence of a central dusty region in which the water molecules can survive? And are these regions destroyed by the more violent process of fueling by mergers? If this is the case, one might expect to find megamasers preferentially in barred galaxies. However, the percentage of barred galaxies in the sample of known megamasers residing in spiral galaxies is with 54% (see above) not higher than what is typically found for the fraction of barred galaxies in the local universe (e.g., Barazza et al. 2008).

[18] However, the axis of the spiral disk seems to be completely uncorrelated with that of the accretion disk as traced by the radio jet (e.g., Schmitt et al. 2002).

6. SUMMARY

We report a search for megamasers in 274 SDSS type-2 AGNs ($0.3 < z < 083$), half of which are luminous enough (in [O III]) to be classified as type-2 QSOs (Zakamska et al. 2003). Apart from the detection of the gigamaser J0804+3607 already reported by Barvainis & Antonucci (2005), we do not find any additional line emission. We estimate the detection probabilities by comparing our sample with known megamasers, taking into account the observed H_2O maser LF and the sensitivity of our survey. We discuss intrinsic differences between the known megamasers, mainly low-luminous AGNs such as Seyfert-2 galaxies and LINERs in the local universe, and our sample consisting of high-luminous AGNs at higher redshift. At this stage, we cannot distinguish between the different scenarios presented that could lead to the high rate of nondetections.

Further and more sensitive observations are required, e.g., using the Square Kilometer Array (SKA). Detecting megamasers in type-2 QSOs remains a challenging and yet, if successful,

highly rewarding project not only to determine BH masses but especially for its possibility of constraining distances and thus the properties of the elusive dark energy.

We thank Neil Nagar for his help with the LF. We thank Phil Perillat and Chris Salter for help with the Arecibo observations and reductions. We thank the anonymous referee for carefully reading the manuscript and for useful suggestions. N.B. is supported through a grant from the National Science Foundation (AST 0507450). The National Radio Astronomy Observatory is a facility of the National Science Foundation operated under cooperative agreement by Associated Universities, Inc. The 100 m radio telescope at Effelsberg is operated by the Max-Planck-Institut für Radioastronomie (MPIR) on behalf of the Max-Planck-Gesellschaft (MPG). The Arecibo Observatory is part of the National Astronomy and Ionosphere Center, which is operated by Cornell University under a cooperative agreement with the National Science Foundation. This research has made use of the NASA/IPAC Extragalactic Database (NED) which is operated by the Jet Propulsion Laboratory, California Institute of Technology, under contract with the National Aeronautics and Space Administration. For the reduction and analysis of the Effelsberg data, we used the GILDAS/CLASS software (http://www.iram.fr/IRAMFR/GILDAS).

APPENDIX

ADDITIONAL OBSERVATIONS

In addition to the SDSS type-2 AGNs, a sample of 76 radio galaxies at $z = 0.3$–0.7 was observed during the same observing runs at the GBT and the Effelsberg 100 m radio telescope (Table 4). An additional sample of high-redshift radio galaxies was observed at Arecibo Observatory (see A1; Table 4). The radio galaxies were selected from objects in NED classified as "galaxy" and "radio source" whose frequencies were accessible to the different telescope receivers and whose declinations were in the observatory range. Also, a few sources classified as galaxy or QSO were observed (26 in total; Table 5).

A.1. Arecibo

A total of 71 objects with $z = 1.1$–3.6 were observed during observing runs in 2003 October and June, 2004 September, and 2005 March in dual polarization, single-beam, position-switching mode (see Table 4). Each observation consisted of typically five on/off scans of 10 minutes each, resulting in a total duration of 50 minutes per source. (However, some objects only have two or three individual scans.) Total spectrometer bandwidths of either 25 MHz or 50 MHz were divided into 1024 channels. Antenna gain, as determined from previous measurements by Arecibo staff, ranged from about 3 K Jy^{-1} to 7 K Jy^{-1}, depending on frequency, and flux calibration was done using these values obtained from a lookup table. We estimate that calibrations are accurate to 20%. Pointing was checked approximately every 2 hr using extragalactic radio sources.

REFERENCES

Antonucci, R. R. J. 1993, ARA&A, 31, 473
Argon, A. L., Greenhill, L. J., Moran, J. M., Reid, M. J., Menten, K. M., Henkel, C., & Inoue, M. 1994, ApJ, 422, 586
Argon, A. L., Greenhill, L. J., Moran, J. M., Reid, M. J., Menten, K. M., & Inoue, M. 2004, ApJ, 615, 702
Argon, A. L., Greenhill, L. J., Reid, M. J., Moran, J. M., & Humphreys, E. M. L. 2007, ApJ, 659, 1040
Bahcall, J. N., Kirhakos, S., Saxe, D. H., & Schneider, D. P. 1997, ApJ, 479, 642
Ball, G. H., Greenhill, L. J., Moran, J. M., Zaw, I., & Henkel, C. 2005, ASPC, 340, 235
Barazza, F. D., Jogee, S., & Marinova, I. 2008, ApJ, 675, 1194
Barth, A. J., Tran, H. D., Brotherton, M. S., Filippenko, A. V., Ho, L. C., van Breugel, W., Antonucci, R., & Goodrich, R. W. 1999, AJ, 118, 1609
Barvainis, R., & Antonucci, R. 2005, ApJ, 628, 89
Baudry, A., & Brouillet, N. 1996, A&A, 316, 188
Becker, R., Henkel, C., Wilson, T. L., & Wouterloot, J. G. A. 1993, A&A, 268, 483
Bennert, N., Canalizo, G., Jungwiert, B., Stockton, A., Schweizer, F., Peng, C. Y., & Lacy, M. 2008, ApJ, 677, 846
Braatz, J. A., & Gugliucci, N. E. 2008, ApJ, 678, 96
Braatz, J. A., Henkel, C, Greenhill, L. J., Moran, J. M., & Wilson, A. S. 2004, ApJ, 617, L29
Braatz, J. A., Wilson, A. S., & Henkel, C. 1994, ApJ, 437, L99
Braatz, J. A., Wilson, A. S., & Henkel, C. 1996, ApJS, 106, 51
Braatz, J. A., Wilson, A. S., & Henkel, C. 1997, ApJS, 110, 321
Braatz, J. A., Wilson, A. S., Henkel, C., Gough, R., & Sinclair, M. 2003, ApJS, 146, 249
Braatz, et al. 2007, in IAU Symp. 242, Astrophysical Masers and their Environments, ed. J. M. Chapman & W. A. Baan (Cambridge: Cambridge Univ. Press) 399
Brunthaler, A., Henkel, C., de Blok, W. J. G., Reid, M. J., Greenhill, L. J., & Falcke, H. 2006, A&A, 457, 109
Brunthaler, A., Reid, M., Falcke, H., Greenhill, L. J., & Henkel, C. 2005, Science, 307, 1440
Canalizo, G., Bennert, N., Jungwiert, B., Stockton, A., Schweizer, F., Lacy, M., & Peng, C. 2007, ApJ, 669, 801
Canalizo, G., & Stockton, A. 2001, ApJ, 555, 719
Castangia, P., Tarchi, A., Henkel, C., & Menten, K. M. 2008, A&A, 479, 111
Churchwell, E., Witzel, A., Huchtmeier, W., Pauliny-Toth, I., Roland, J., & Sieber, W. 1977, A&A, 54, 969
Claussen, M. J., Diamond, P. J., Braatz, J. A., Wilson, A. S., & Henkel, C. 1998, ApJ, 500, L129
Claussen, M. J., Heiligman, G. M., & Lo, K. Y. 1984, Nature, 310, 298
Combes, F. 2006, RevMexAA, 26, 131
Condon, J. J. 1989, ApJ, 338, 13
Darling, J., & Giovanelli, R. 2002, ApJ, 572, 810
Disney, M. J., et al. 1995, Nature, 376, 150
Dos Santos, P. M., & Lépine, J. R. D. 1979, Nature, 278, 34
Falcke, H., Henkel, C., Peck, A. B., Hagiwara, Y., Prieto, A. M., & Gallimore, J. F. 2000a, A&A, 358, L17
Falcke, H., Wilson, A. S., Henkel, C., Brunthaler, A., & Braatz, J. A. 2000b, ApJ, 530, 13
Floyd, D. J. E., Kukula, M. J., Dunlop, J. S., McLure, R. J., Miller, L., Percival, W. J., Baum, S. A., & O'Dea, C. P. 2004, MNRAS, 355, 196
Fullmer, L., & Lonsdale, C. J. 1989, Cataloged Galaxies and Quasars Observed in the IRAS Survey, Version 2 (Pasadena: Jet Propulsion Laboratory)
Gallimore, J. F., Henkel, C., Baum, S. A., Glass, I. S., Claussen, M. J., Prieto, M. A., & von Kap-Herr, S. 2001, ApJ, 556, 694
Gardner, F. F., & Whiteoak, J. B. 1982, MNRAS, 201, 13
Greenhill, L. J. 2004, New Astron. Rev., 48, 1079
Greenhill, L. J., Ellingsen, S. P., Norris, R. P., Gough, R. G., Sinclair, M. W., Moran, J. M., & Mushotzky, R. 1997b, ApJ, 474, L103
Greenhill, L. J., Herrnstein, J. R., Moran, J. M., Menten, K. M., & Velusamy, T. 1997a, ApJ, 486, L15
Greenhill, L. J., Jiang, D. R., Moran, J. M., Reid, M. J., Lo, K. Y., & Claussen, M. J. 1995, ApJ, 440, 619
Greenhill, L. J., Kondratko, P. T., Lovell, J. E. J., Kuiper, T. B. H., Moran, J. M., Jauncey, D. L., & Baines, G. P. 2003a, ApJ, 582, L11
Greenhill, L. J., Moran, J. M., Reid, M. J., Menten, K. M., & Hirabayashi, H. 1993, ApJ, 406, 482
Greenhill, L. J., Tilak, A., & Madejski, G. 2008, ApJ, 686, L13
Greenhill, L. J., et al. 2002, ApJ, 565, 836
Greenhill, L. J., et al. 2003b, ApJ, 590, 162
Guyon, O., Sanders, D. B., & Stockton, A. 2006, ApJS, 166, 89
Hagiwara, Y., Diamond, P. J., & Miyoshi, M. 2002, A&A, 383, 65
Hagiwara, Y., Diamond, P. J., & Miyoshi, M. 2003a, A&A, 400, 457
Hagiwara, Y., Diamond, P. J., Miyoshi, M., Rovilos, E., & Baan, W. A. 2003b, MNRAS, 344, L53
Hagiwara, Y., Diamond, P. J., Nakai, N., & Kawabe, R. 2001a, ApJ, 560, 119
Hagiwara, Y., Henkel, C., Menten, K. M., & Nakai, N. 2001b, ApJ, 560, L37
Hagiwara, Y., Kohno, K., Kawabe, R., & Nakai, N. 1997, PASJ, 49, 171
Haschick, A. D., & Baan, W. A. 1985, Nature, 314, 144

Henkel, C., Braatz, J. A., Greenhill, L. J., & Wilson, A. S. 2002, A&A, 394, L23
Henkel, C., Braatz, J. A., Tarchi, A., Peck, A. B., Nagar, N. M., Greenhill, L. J., Wang, M., & Hagiwara, Y. 2005b, Ap&SS, 295, 107
Henkel, C., Güsten, R., Downes, D., Thum, C., Wilson, T. L., & Biermann, P. 1984, A&A, 141, L1
Henkel, C., Peck, A. B., Tarchi, A., Nagar, N. M., Braatz, J. A., Castangia, P., & Moscadelli, L. 2005a, A&A, 436, 75
Henkel, C., Tarchi, A., Menten, K. M., & Peck, A. B. 2004, A&A, 414, 117
Henkel, C., Wang, Y. P., Falcke, H., Wilson, A. S., & Braatz, J. A. 1998, A&A, 335, 463
Henkel, C., Wouterloot, J. G. A., & Bally, J. 1986, A&A, 155, 193
Herrnstein, J. R., Moran, J. M., Greenhill, L. J., & Trott, A. S. 2005, ApJ, 629, 719
Herrnstein, J. R., et al. 1999, Nature, 400, 539
Ho, P. T. P., Martin, R. N., Henkel, C., & Turner, J. L. 1987, ApJ, 320, 663
Huchtmeier, W. K., Eckart, A., & Zensus, A. J. 1988, A&A, 200, 26
Huchtmeier, W. K., Witzel, A., Khr, H., Pauliny-Toth, I. I., & Roland, J. 1978, A&A, 64, L21
Humphreys, E. M. L., Reid, M. J., Greenhill, L. J., Moran, J. M., & Argon, A. L. 2008, ApJ, 672, 800
Hutchings, J. B., Holtzman, J., Sparks, W. B., Morris, S. C., Hanisch, R. J., & Mo, J. 1994, ApJ, 429, L1
Ishihara, Y., Nakai, N., Iyomoto, N., Makishima, K., Diamond, P., & Hall, P. 2001, PASJ, 53, 2151
Koekemoer, A. M., Henkel, C., Greenhill, L. J., Dey, A., van Breugel, W., Codella, C., & Antonucci, R. 1995, Nature, 378, 697
Kondratko, P. T., Greenhill, L. J., & Moran, J. M. 2006a, ApJ, 652, 136
Kondratko, P. T., et al. 2006b, ApJ, 638, 100
Labita, M., Treves, A., Falomo, R., & Uslenghi, M. 2006, MNRAS, 373, 551
Lo, K. Y. 2005, ARA&A, 43, 625
Maiolino, R., Risaliti, G., & Salvati, M. 1999, A&A, 341, L35
Malkan, M. A., Gorjian, V., & Raymond, T. 1998, ApJS, 117, 25
McLure, R. J., Kukula, M. J., Dunlop, J. S., Baum, S. A., O'Dea, C. P., & Hughes, D. H. 1999, MNRAS, 308, 377
Miyoshi, M., Moran, J. M., Herrnstein, J. R., Greenhill, L., Nakai, N., Diamond, P., & Inoue, M. 1995, Nature, 373, 127
Morganti, R., Greenhill, L. J., Peck, A. B., Jones, D. L., & Henkel, C. 2004, New Astron. Rev., 48, 1195
Nakai, N., Sato, N., & Yamauchi, A. 2002, PASJ, 54, L27
Neufeld, D. A. 2000, ApJ, 542, L99
Neufeld, D. A., Maloney, P. R., & Conger, S. 1994, ApJ, 436, L127
Ott, M., Witzel, A., Quirrenbach, A., Krichbaum, T. P., Standke, K. J., Schalinski, C. J., & Hummel, C. A. 1994, A&A, 284, 331
Peck, A. B., Henkel, C., Ulvestad, J. S., Brunthaler, A., Falcke, H., Elitzur, M., Menten, K. M., & Gallimore, J. F. 2003, ApJ, 590, 149
Reid, M. J., Braatz, J. A., Condon, J. J., Greenhill, L. J., Henkel, C., & Lo, K. Y. 2008, arXiv:0811.4345v1
Schmidt, M. 1968, ApJ, 151, 393
Schmitt, H. R., Pringle, J. E., Clarke, C. J., & Kinney, A. L. 2002, ApJ, 575, 150
Simpson, C. 2005, MNRAS, 360, 565
Solomon, P. M., & Vanden Bout, P. A. 2005, ARA&A, 43, 677
Tarchi, A., Brunthaler, A., Henkel, C., Menten, K. M., Braatz, J., & Weiß, A. 2007, A&A, 475, 497
Tarchi, A., Henkel, C., Chiaberge, M., & Menten, K. M. 2003, A&A, 407, L33
Tarchi, A., Henkel, C., Peck, A. B., & Menten, K. M. 2002a, A&A, 385, 1049
Tarchi, A., Henkel, C., Peck, A. B., & Menten, K. M. 2002b, A&A, 389, L39
Trotter, A. S., Greenhill, L. J., Moran, J. M., Reid, M. J., Irwin, J. A., & Lo, K.-Y. 1998, ApJ, 495, 740
Urrutia, T., Lacy, M., & Becker, R. H. 2008, ApJ, 674, 80
Veron-Cetty, M.-P., & Veron, P. 1996, ESO Sci. Rep., 17, 1
Vestergaard, M., Fan, X., Tremonti, C. A., Osmer, P. S., & Richards, G. T. 2008, ApJ, 674, L1
Vignali, C., Brandt, W. N., & Schneider, D. P. 2003, AJ, 125, 433
Wilkes, B. J., Schmidt, G. D., Smith, P. S., Mathur, S., & McLeod, K. K. 1995, ApJ, 455, 13
Wilson, A. S., Braatz, J. A., & Henkel, C. 1995, ApJ, 455, L127
Wouterloot, J. G. A., & Walmsley, C. M. 1986, A&A, 168, 237
Wright, E. L. 2006, PASP, 118, 1711
Zakamska, N. L., Strauss, M. A., Heckman, T. M., Ivezic, Z., & Krolik, J. H. 2004, AJ, 128, 1002
Zakamska, N. L., et al. 2003, AJ, 126, 2125
Zakamska, N. L., et al. 2005, AJ, 129, 1212
Zakamska, N. L., et al. 2006, AJ, 132, 1496
Zhang, J. S., Henkel, C., Kadler, M., Greenhill, L. J., Nagar, N., Wilson, A. S., & Braatz, J. A. 2006, A&A, 450, 933